Robust Vehicle Lateral Stabilization via Set-Based Methods for Uncertain Piecewise Affine Systems: Experimental Results

Giovanni Palmieri, Miroslav Barić, Luigi Glielmo, Eric H. Tseng and Francesco Borrelli

Abstract— The paper presents the design of a lateral stability controller for ground vehicles based on front steering and four wheels independent braking. The control objective is to track yaw rate and lateral velocity reference signals while avoiding front and rear wheel traction force saturation. Control design is based on an approximate piecewise–affine nonlinear dynamical model of the vehicle. Vehicle longitudinal velocity and driver steering input are modeled as measured disturbances taking values in a compact set.

We use a time-optimal control strategy which ensures convergence into a maximal robust control invariant set. This paper presents the controller experimental results on a vehicle equipped with active front steering and differential braking. In particular, tests at high-speed on ice with aggressive driver maneuvers show the effectiveness of the proposed scheme.

I. INTRODUCTION

In our previous work ([9],[8],[10]) we presented a systematic approach to design yaw and lateral dynamics control using the coordination of active front steering with differential braking. We modeled the nonlinear dynamics of vehicle as a PWA discrete–time system, whose states (yaw rate and lateral velocity) and control variables (front turn wheel angle and braking moment) are subject to hard constraints. Longitudinal velocity is treated as a state–dependent measured disturbance. In [10] we introduced a controller which guarantees constraints satisfaction at all times for all possible disturbance realizations captured by the model. Due to the presence of hard constraints and strict constraint satisfaction requirements, we base our design on *set–theoretic methods* (cf. [3]). In particular, we characterize and compute the robust control invariant (RCI) set for the piecewise–affine model of the vehicle using the results on *Min–max* and *Max–min reachability*, introduced respectively in [12] and [13], [1]. Such RCI set serves as a foundation for time–optimal robust control strategy. In this work we validate the controller introduced in [10] in an experimentally study with two main objectives in mind. First, our goal is to verify the validity of the simplified vehicle and disturbance models used in [10] and based on that to infer (or disprove) the validity of the guarantees provided by the proposed robust control design. Secondly, we would like to evaluate the performance of the proposed control strategy when tested in closed loop with the driver.

G. Palmieri and L.Glielmo are with Engineering Department of Universitá degli Studi del Sannio, 82100 Benevento, Italy. G.Palmieri is the corresponding author palmieri@unisannio.it

F. Borrelli and M. Barić are with Department of Mechanical Engineering, University of California, Berkeley, 94720-1740, U.S.A. M. Barić is currently at the United Technologies Research Center, East Hartford, CT 06108, U.S.A.

H. E. Tseng is with Ford Research Laboratories, Dearborn, MI, U.S.A.

The paper is structured as follows. In Section II we present the vehicle model. Starting from the classical nonlinear bicycle model, we obtain a Piecewise Affine (PWA) realization. In Section III, we present the controller design. Experimental results are reported in Section IV followed by final remarks in Section V. Sections II–III have been extracted from [9], [8], [10].

II. A MODEL OF THE LATERAL VEHICLE DYNAMICS

In this section, starting from the standard nonlinear bicycle model [11, Sec. 2.3] we describe the Hybrid PieceWise Affine (HPWA) bicycle model used for robust controller synthesis. We use the following notation: the subscripts $(\cdot)_f$ and $(\cdot)_r$ denote variables associated with the front and the rear wheel, respectively. Also, the subscript $()_\star$ stands for both $(\cdot)_f$ and $(\cdot)_r$.

The *bicycle model* (cf. [5], [11]) is given by

$$m\ddot{y} = -m\dot{x}\dot{\psi} + 2F_{c_f} + 2F_{c_r}, \tag{1a}$$

$$I\ddot{\psi} = 2aF_{c_f} - 2bF_{c_r} + M, \tag{1b}$$

where $\dot{y}$ is the lateral speed, $\dot{x}$ is the longitudinal velocity, $\dot{\psi}$ is the yaw rate, M is the braking moment, $F_{c_\star}$ are the cornering tire forces, a is longitudinal distance from the vehicle's center of gravity (CoG) to the front axle, b is longitudinal distance from CoG to the rear axle and I is yaw inertia moment of vehicle around the z-axis.

For cornering tire forces we are using the well-known *Pacejka's model* ([7]), where they are defined by a *static non–linear mapping*:

$$F_{c_\star} = f_c(\alpha_\star, s_\star, \mu_\star, F_{z_\star}), \tag{2}$$

with $s_\star$ slip ratios (the normalized difference between the longitudinal slip velocity and the forward speed of the wheel center [7, Sec. 2.2]), μ the friction coefficient, $\alpha_\star$ tire slip angles and $F_{z\star}$ normal tire forces. The dependence of the cornering (lateral) tire force on the slip angle α, for a fixed value of the slip ration $s = 0$, is depicted in Figure 1. Most of the practical set–theoretic based control synthesis methods rely on polytopic set representations. In that respect, a suitable model for nonlinear system dynamics is a *piecewise-affine (PWA) model*. PWA models are also particulary amenable for approximation of cornering Pacejka tire forces shown in Figure 1.

We introduce the following assumption.

Assumption 1: The friction coefficient μ is known, constant and equal for both wheels of the bicycle model. Normal tire forces $F_{z\star}$ are assumed to be constant, known and the same for both wheels.

Fig. 1. Lateral tire force.

S 1	$z_1 \geq 0$	$z_2 \geq 0$	$w_{z_1} \geq v_{x_{\max}} z_1 - T_s v_{x_{\min}}^2 z_2$ $w_{z_1} \leq v_{x_{\min}} z_1 - T_s v_{x_{\max}}^2 z_2$ $z_1 \leq z_{1_{\max}}$ $z_2 \leq z_{2_{\max}}$
S 2	$z_1 \leq 0$	$z_2 \geq 0$	$w_{z_1} \geq v_{x_{\min}} z_1 - T_s v_{x_{\min}}^2 z_2$ $w_{z_1} \leq v_{x_{\max}} z_1 - T_s v_{x_{\max}}^2 z_2$ $z_1 \geq z_{1_{\min}}$ $z_2 \leq z_{2_{\max}}$
S 3	$z_1 \geq 0$	$z_2 \leq 0$	$w_{z_1} \geq v_{x_{\min}} z_1 - T_s v_{x_{\min}}^2 z_2$ $w_{z_1} \leq v_{x_{\max}} z_1 - T_s v_{x_{\max}}^2 z_2$ $z_1 \leq z_{1_{\min}}$ $z_2 \geq z_{2_{\max}}$
S 4	$z_1 \leq 0$	$z_2 \leq 0$	$w_{z_1} \leq v_{x_{\min}} z_1 - T_s v_{x_{\max}}^2 z_2$ $w_{z_1} \geq v_{x_{\max}} z_1 - T_s v_{x_{\min}}^2 z_2$ $z_1 \geq z_{1_{\min}}$ $z_2 \geq z_{2_{\min}}$

TABLE I
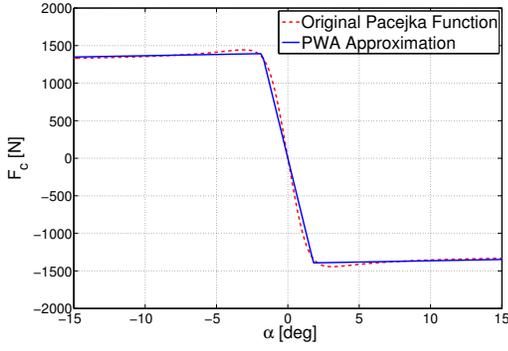
Under the above assumptions, it is reasonable to consider $F_{c\star}$ in their pure cornering condition ($s_\star = 0$) and depending only on the slip angles $\alpha_\star$. The dependence of forces $F_{c\star}$ on the states $\dot{y}$, $\dot{\psi}$ is derived as follows. First, we consider, under small angles approximation, the linear state–input combination to describe front and rear tire slip angle α_f and α_r:

$$\alpha_f = \frac{a\dot{\psi} + \dot{y}}{\dot{x}} - \delta_f, \quad \alpha_r = \frac{b\dot{\psi} - \dot{y}}{\dot{x}}. \quad (3)$$

From equations (3) it is possible model the lateral force as the piecewise affine function

$$g_\star(\alpha_\star) = \begin{cases} c_s\alpha_\star + (c_l + c_s)\alpha_\star^\bullet, & \text{if } -\frac{\pi}{6} \leq \alpha_\star \leq -\alpha_\star^\bullet, \\ -c_l\alpha_\star, & \text{if } -\alpha_\star^\bullet \leq \alpha_\star \leq \alpha_\star^\bullet, \\ c_s\alpha_\star - (c_l + c_s)\alpha_\star^\bullet, & \text{if } \alpha_\star^\bullet \leq \alpha_\star \leq \frac{\pi}{6}, \end{cases} \quad (4)$$

where the interval $[-\alpha_\star^\bullet, \alpha_\star^\bullet]$ is the linear region, the interval $[-\pi/6, -\alpha_\star^\bullet]$ is the region of force negative saturation and the interval $[\alpha_\star^\bullet, \pi/6]$ is the region of force positive saturation.

For the longitudinal velocity, we assume the following:

Assumption 2: The longitudinal velocity of the vehicle v_x is bounded within the interval $[v_x^{\min}, v_x^{\max}]$ and is known (measured) at every discrete–time instant.

Substituting equations (4) into (1), we obtain the hybrid (PWA) bicycle model of the vehicle:

$$\dot{\xi} = \begin{bmatrix} a_{11} & a_{12} \\ a_{21} & a_{22} \end{bmatrix}_i \frac{\xi}{v_x} + \begin{bmatrix} 0 & -v_x^2 \\ 0 & 0 \end{bmatrix} \frac{\xi}{v_x} + B_i u + f_i. \quad (5)$$

where $\xi = [\dot{y}, \dot{\psi}]^T$, $u = [\delta_f, M]^T$ and $v_x = \dot{x}$. We define:

$$\bar{A}_i := \begin{bmatrix} a_{11} & a_{12} \\ a_{21} & a_{22} \end{bmatrix}_i, \quad z := \frac{\xi}{v_x} \quad (6)$$

$$w_1 := -v_x^2 z_2, \quad \bar{B}_i := B_i = \begin{bmatrix} b_{11} & 0 \\ b_{21} & b_{22} \end{bmatrix}_i,$$

$$\bar{f}_i := f_i$$

to obtain the compact representation of system (5)

$$\dot{\xi} = \bar{A}_i z + \begin{bmatrix} 1 \\ 0 \end{bmatrix} w_1 + \bar{B}_i u + \bar{f}_i. \quad (7)$$

Using Euler's method we can discretize the model (6)–(7)

$$\xi(k+1) = \hat{A}_i z(k) + \hat{B}_i u(k) + \hat{f}_i + w_z(k), \quad (8)$$

where $w_z(k) := T_s \begin{bmatrix} 1 \\ 0 \end{bmatrix} w_1(k) + \xi(k)$. In model (8) the evolution of the state vector ξ is defined by the linear expression in $z = \xi/v_x$, whose value is known at each time instant.

Using the definition of z in (6), we can rewrite the equation (3) as follows:

$$\alpha_f = az_2 + z_1 - \delta_f, \quad \alpha_r = bz_2 - z_1. \quad (9)$$

The constraints on z given by (4) and (9) are polygonal sets. Table I reports the bounds on the first component of the disturbance w_{z_1}, while w_{z_2} satisfies the following linear inequalities:

$$z_2^{\min} \leq z_2, \quad \leq z_2^{\max}, v_x^{\max} z_2 - w_{z_2} \leq 0. \quad (10)$$

The reader can find the details construction of bounds in Table I and (10) in [8] and [10]. The equations (4), (8) and (9) provide a hybrid dynamical system with nine modes. In each mode the system dynamics is affine. The mode selection depends on the side slip angles $\alpha_\star$ according to (4). By using the equations (9), the hybrid bicycle model (8) can be compactly written as

$$\xi^+ = \hat{A}_i z + \hat{B}_i u + \hat{f}_i + w_z,$$
$$(z, u) \in \mathcal{Q}_i, \quad w_z \in \mathcal{W}_z(z) \quad i \in \{1, \dots, 9\}, \quad (11)$$

where $z = [\frac{\dot{y}}{v_x}; \frac{\dot{\psi}}{v_x}]^T$, $\{\mathcal{Q}_i\}_{i=1}^9$ is a collection of *polyhedral regions* in $\mathbb{R}^4$ defining the regions for each dynamic behavior and *constraints on the scaled state and control variables*, and $\mathcal{W}_z(\cdot)$ is a set-valued mapping. In addition to the speed uncertainty captured by w_z, in this paper we also consider an *uncertainty in the actuation* by extending the hybrid bicycle model (11) with an uncertainty term w_u. The resulting model is

$$\xi^+ = \hat{A}_i z + \hat{B}_i u + \hat{f}_i + w_z + w_u,$$
$$(z, u) \in \mathcal{Q}_i, \quad w_z \in \mathcal{W}_z(z), \quad w_u \in \mathcal{W}_u(u) \quad (12)$$

where $\mathcal{W}_u(\cdot)$ is a set-valued mapping. Differently from w_z, at every sampling time the value of the uncertainty w_u is *not known to the controller*. The controller, however, is aware of the bounds on w_u and assumes that w can take *an arbitrary value* within the set $\mathcal{W}(u)$.

In this work we assume that each of the control inputs, the steering δ_f and the braking moment M, is affected by $\pm 10\%$ uncertainty in its value.

III. ROBUST CONTROL COMPUTATION

In this section we describe the robust control strategy *for all possible variations of the longitudinal velocity v_x and for all possible realizations of the input uncertainties w_u*. The controller design aims primarily at inducing the "nominal" behavior of the vehicle, i.e., dynamic behavior obtained when neither front nor rear tires are saturated and, at the same time, tracking the given reference vector r as close as possible.

We formalize these notions via robust control invariance and constrained controllability for the considered system class affected by input–dependent uncertainties. We provide only very limited discussion on these topics. For supplementary details the reader is referred to [12], [13], [1], [10]. Rewrite system (12) compactly as:

$$\xi^+ = f_{pwa}(z, u, w_z, w_u), \tag{13a}$$
$$(z, u) \in \mathcal{C}_{zu}, w_z \in \mathcal{W}_z(z), w_u \in \mathcal{W}_u(u) \tag{13b}$$

and consider the one–step robust backwards–reachable set given by the following mapping:

$$Pre_\xi(\mathcal{X}) := \Big\{ \xi \colon \forall w_z \in \mathcal{W}_z(z) \, \exists u \text{ such that } (z, u) \in \mathcal{C}_{zu}$$
$$\text{and } f_{pwa}(\frac{\xi}{v_x}, u, w_z, w_u) \in \mathcal{X}, \forall w_u \in \mathcal{W}_u(u) \Big\}.$$

The set $Pre_\xi(\mathcal{X})$ can be computed as follows. First the one–step robust backwards–reachable set $Pre_z(\mathcal{X})$ is computed for the system

$$z^+ = f_{pwa}(z, u, w_z, w_u), \tag{14a}$$
$$(z, u) \in \mathcal{C}_{zu}, w_z \in \mathcal{W}_z(z), w_u \in \mathcal{W}_u(u), \tag{14b}$$

using the combinations of algorithms introduced in [12] and [13], [1] and subsequently applied in [10]. Then, we compute the set $Pre_\xi(\mathcal{X})$ as

$$Pre_\xi(\mathcal{X}) = \Omega_\xi \backslash \text{Proj}_\xi \left(\left\{ \Omega_{\xi v_x} \backslash \bigcup_{i=1}^{q} \mathcal{P}_i^{\xi v_x} \right\} \right), \tag{15}$$

where $\Omega_\xi := \text{Proj}_\xi(\mathcal{C}_{\xi u})$, $\Omega_{\xi v_x} := \Omega_\xi \times \mathcal{V}_x$ and the sets $\mathcal{C}_{\xi u}$ and $\mathcal{V}_x$ are the constraint sets as specified in (12). Again, for details of the algorithms and the expression (15) interested reader is referred to [10] and references therein.

Operations on sets required to perform computations in (15) for polygonal constraints and target set $\mathcal{X}$ have been performed by using the MPT Toolbox (cf. [6]). Thus the mapping $Pre_\xi(\cdot)$ for the case of polygonal argument sets and constraints can be readily implemented and used for the computation of the robust *max–min* controller, as discussed next.

The primary task of the Robust ESC (RESC) controller we are going to design next is to preserve "nominal" behavior of the car for all possible values w_z considered in the design. Let us enumerate the polyhedral regions $\mathcal{Q}_i$ of our PWA model (12) so that the vehicle is in the linear mode at time k if $(z_k, u_k) \in \mathcal{Q}_1$. For this reason we refer to the linear regime of the tires as "mode 1". In our discrete–time setting, the desired control action u_k at any time instant k must satisfy $(z_k, u_k) \in \mathcal{Q}_1$ and at the same time $\xi_{k+1}/v_x(k+1) \in \text{Proj}_z(\mathcal{Q}_1)$ *for all possible $v_x(k+1)$*, i.e. for all $v_x(k+1) \in \mathcal{V}_x$. Let

$$\text{Proj}_z(\mathcal{Q}_1) = \left\{ z \colon H^1 z \le k^1 \right\},$$

and define $\mathcal{P}_1$ as follows:

$$\mathcal{P}_1 = \{ \xi \colon H^1 \xi \le k^1 v_x^{\min} \} \cap \{ \xi \colon H^1 \xi \le k^1 v_x^{\max} \}. \tag{16}$$

We formalize the notion of robustness to velocity variations by defining *mode 1 robust control invariant (RCI)* set:

Definition 1: A set $\mathcal{R} \subseteq \mathcal{P}_1$ is called *mode 1 RCI set* for the dynamical system (12) if for every $\xi \in \mathcal{R}$ and each $(v_x, w_z) \in \mathcal{V}_x \times \mathcal{W}_z(\xi/v_x)$ there exists a control u such that $(\xi/v_x, u) \in \mathcal{Q}_1$ and $\hat{A}_1 \xi/v_x + \hat{B}_1 u + \hat{f}_1 + w_z + w_z \in \mathcal{R}$ for all $w_u \in \mathcal{W}_u(u)$.

For our purposes it is desirable to characterize the maximal mode 1 RCI set $\mathcal{R}_\infty^1$ which contains all other mode 1 RCI sets and can be obtain using the standard iterative procedure given by Algorithm introduced in [2]. In the Algorithm we perform computations of backwards–reachable sets only for the constraints and the dynamics associated to the mode 1. In particular, the mapping $Pre_\xi^1(\cdot)$ is given by:

$$Pre_z^1(\mathcal{X}) := \{ z \colon \forall w_z \in \mathcal{W}_z(z) \, \exists u \text{ such that } (z, u) \in \mathcal{Q}_1$$
$$\text{and } \hat{A}_1 z + \hat{B}_1 u + \hat{f}_1 + w_z + w_z \in \mathcal{X}$$
$$\forall w_u \in \mathcal{W}_u(u) \}$$
$$Pre_\xi^1(\mathcal{X}) := \left\{ \xi \colon \frac{\xi}{v_x} \in Pre_z^1(\mathcal{X}), \forall v_x \in \mathcal{V}_x \right\}.$$

If Algorithm [2] terminates in finitely many iterations i_t, then the set $\mathcal{R}_\infty^1 = \mathcal{X}_{i_t}$.

To the set $\mathcal{R}_\infty^1$ we associate the control mapping $\mathcal{U}_\infty^1(\cdot)$ non–empty for all $\xi \in \mathcal{R}_\infty^1$ and all $v_x \in \mathcal{V}_x$:

$$\mathcal{U}_\infty^1(z, w_z) = \{ u \colon (z, u) \in \mathcal{Q}_1 \text{ and } \forall w_u \in \mathcal{W}_u(u)$$
$$\hat{A}_1 z + \hat{B}_1 u + \hat{f}_1 + w_z + w_u \in \mathcal{R}_\infty^1 \}. \tag{17}$$

For a given scaled state vector z, any control input selected from the set $\mathcal{U}_\infty^1(z)$ results in the successor state ξ^+ being inside the set $\mathcal{R}_\infty^1$.

The maximal mode 1 RCI set is robust to the modeled uncertainties w_z and w_u. The Robust ESC controller can keep the state trajectory within the set $\mathcal{R}_\infty^1$ using braking and steering wheel angle for all admissible values of w_z and w_u. Also, the RESC may be activated by the driver at the moment when the state $\xi \notin \mathcal{R}_\infty^1$, e.g. when the vehicle is over-steering or under-steering. In such situations the RESC

scheme should bring the state back to the set $\mathcal{R}_\infty^1$. For that purpose we compute the k–step controllable sets $\mathcal{X}_k$, $k \leq 2$:

$$\mathcal{X}_k = Pre_\xi(\mathcal{X}_{k-1}), \; k = 1, \ldots, N, \tag{18}$$

with $\mathcal{X}_0 = \mathcal{R}_\infty^1$. Note that in (18) the control horizon N is chosen by the user trading off the size of the controllable set and the controller computational load. To each controllable set $\mathcal{X}_k$, $k = 1, \ldots, N$, we associate the control mapping:

$$\begin{aligned} \mathcal{U}_k(z, w_z) = \{u : (z, u) \in \mathcal{C}_{zu} \text{ and} \\ f_{pwa}(z, u, w_z, w_u) \in \mathcal{X}_{k-1} \; \forall \; w_u \in \mathcal{W}_u(u)\}. \end{aligned} \tag{19}$$

The value of the mapping $\mathcal{U}_k(\cdot)$ is non–empty for all $\xi \in \mathcal{X}_k$ and for all $v_x \in \mathcal{V}_x$. Figure 2 shows the outcome of the developed control design algorithm for the proposed vehicle model with tire–road friction coefficient $\mu = 0.3$ and the longitudinal velocity range $\mathcal{V}_x = [40, 50]$ [km/h] and the k–step controllable sets $\mathcal{X}_k$ for $k \leq 2$. All the computations
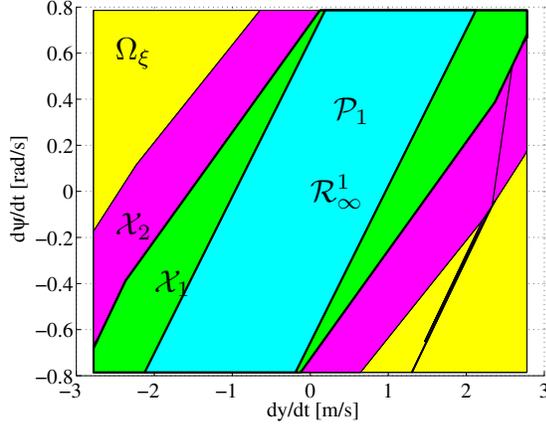
Fig. 2. Robust Control Invariant (RCI) set and 2–step controllable sets $\mathcal{X}_k$ for $\mu = 0.3$ and $40 \leq v_x \leq 50$ [km/h].

briefly outlined above are performed using Multi–Parametric Toolbox for Matlab [6].

A. Implementation Details

The control scheme used in experimental test is a modification of the classical ESC scheme. The "Vehicle" through its sensors transmits the information on its dynamics to "Reference Generator". The controller "RESC" generates appropriate steering and braking control values in order to track the references provided by the "Reference generator" block; while keeping the state trajectory within the set $\mathcal{R}_\infty^1$ or driving it into $\mathcal{R}_\infty^1$. The control input u^* of the "RESC" is computed as:

$$u^* = \arg \min_{u \in \mathcal{U}_\sharp(z, w_z)} (\xi^+ - r)^T Q(\xi^+ - r) + u^T R u, \tag{20}$$

where Q and R are suitably chosen matrices. The actual set of admissible control inputs $\mathcal{U}_\sharp(z, w_z) = \mathcal{U}_k(z, w_z)$ is defined by the mappings (17) and (19); if the state ξ belongs to $\mathcal{R}_\infty^1$, then $\mathcal{U}_\sharp(z, w_z) = \mathcal{U}_\infty^1(z, w_z)$, otherwise $\mathcal{U}_\sharp(z, w_z) = \mathcal{U}_{\bar{k}}(z, w_z)$ with $\bar{k}$ being the smallest k for which $\mathcal{U}_k(z, w_z)$ is non–empty. As the PWA state–update mapping as well as

the set–valued mapping $\mathcal{W}_z(z)$ in (12) are continuous and all constraint sets are compact, the mappings $\mathcal{U}_\infty^1(\cdot)$ and $\mathcal{U}_k(\cdot)$ are compact–valued.

In the proposed setup, $\mathcal{U}_\infty^1(\cdot)$ and $\mathcal{U}_k(\cdot)$, $k = 1, \ldots, N$ are the union of several polytopes. At every sampling time computing u^* amounts to solve a number of optimal control problems. First, we determine the number of polytopes (among $\mathcal{U}_\infty^1(\cdot)$ or $\mathcal{U}_{\bar{k}}(z, w_z)$) containing the measured couple (z, w_z), and then we solve an equal number of optimal problems to compute the u^* with associated minimum cost.

The optimal control solution u^* has two components: the steering wheel angle $u^*(1)$ and the braking moment $u^*(2)$. Both components have to be transformed into front wheel angle command and wheel braking torques, respectively. The total road turn wheel angle δ_{Road} is $\delta_{\text{Road}} = \delta_{\text{AFS}} + \delta_{\text{Driver}}$. The designed control strategy computes the optimal road turn wheel angle, therefore

$$\delta_{\text{AFS}} = u^*(1) - \delta_{\text{Driver}}. \tag{21}$$

We remark that in this study the AFS dynamics (which can be noticed for high values of desired δ_{AFS}) have not been modeled. The wheel braking torques have been computed from $u^*(2)$ by using the algorithm presented in [4].

B. Experimental Setup

We tested the RESC controller on a prototype Jaguar S. In particular, body frame information (lateral and longitudinal velocity, and yaw rate) is measured by the Oxford Technical Solution (OTS) RT3002 sensing system while the actuators are the Active Front Steering (AFS) and a differential braking systems. The computing system is a dSPACE ©Rapid Prototyping (RP).

IV. EXPERIMENTAL RESULTS

In this section, the proposed control strategy is validated through two experiments.

The first experiment shows that the control strategy is robust to longitudinal velocity variation $v_x \in [v_x^{\min}, v_x^{\max}]$ and to input dependent disturbances $w_u \in \mathcal{W}(u)$. We performed a manoeuvre where the car is moving on an icy asphalt ($\mu = 0.3$) and the driver imposes a "smooth" sinusoidal steering profile changing the position of accelerator pedal, such that the car is subject to both decelerations and accelerations as shown in Figure 3.

The tuning parameters are: N = 3; sampling time $T_s = 50ms$; the control weight matrix for the states variable ξ, when the car is inside $\mathcal{R}_\infty^1$, is a diagonal matrix $\text{diag}\,[100, 100]$; while when it is outside is $\text{diag}\,[0.1, 0.1]$, the control weight matrix R, when the car is inside $\mathcal{R}_\infty^1$, is $\text{diag}\,[5 \cdot 10^{-2}, 5 \cdot 10^{-3}]$ while outside it is $\text{diag}\,[5, 5 \cdot 10]$. The vehicle response is shown in Figures 4–5. Tracking performance can be seen in Figure 4 which shows the evolution of the yaw rate and lateral velocity in respect to the generated references. A satisfactory tracking performance is achieved even in the presence of significant lateral speed variations (Figure 4, bottom). The controller is able to produce control inputs, such that both front and rear side slip angles remain
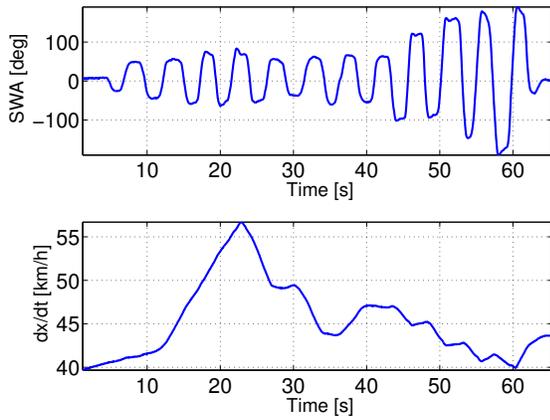
Fig. 3. From the top: driver turn wheel angle δ_d in [deg] and vehicle longitudinal velocity in [km/h]

within their bounds of linear region. State trajectories remain confined within the RCI set $\mathcal{R}_\infty^1$ as it is depicted in Figure 5. Since the proposed controller is always active, it is also
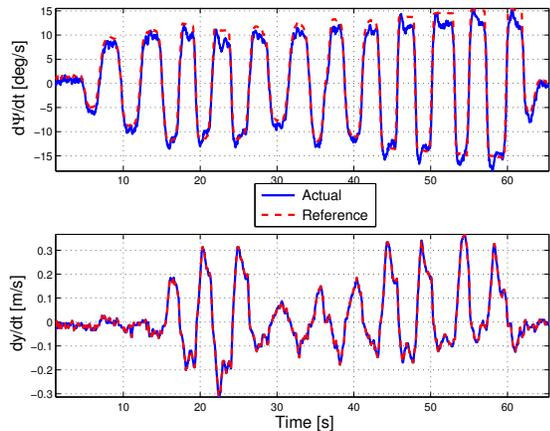
Fig. 4. Experiment 1: From the top: a) reference yaw rate (dashed line) and vehicle yaw rate (solid line); b) reference lateral speed (dashed line) and vehicle lateral speed [km/h] .

important to investigate the interaction between the driver and the controller, i.e. the sensation the controller induces, through braking and steering correction, on the driver. In Figure 6 the turn wheel angle imposed by the driver and the real turn wheel angle after the controller correction are illustrated in the top plot. It is evident that in the beginning (command driver under 5 [deg]) the controller does not intervene by leaving the control to the driver. When the driver performs a sudden turn, the controller creates both the steering and braking correction (Figure 6) in order to preserve tracking of the reference signals while keeping the state trajectories within the set $\mathcal{R}_\infty^1$.

In the second experiment we tested the robustness of the control strategy for more aggressive driver manoeuvres which violate the disturbance bounds accounted for in our design. In this case, the driver imposes a similar sinusoidal steering profile of experiment one on an icy asphalt ($\mu = 0.3$)
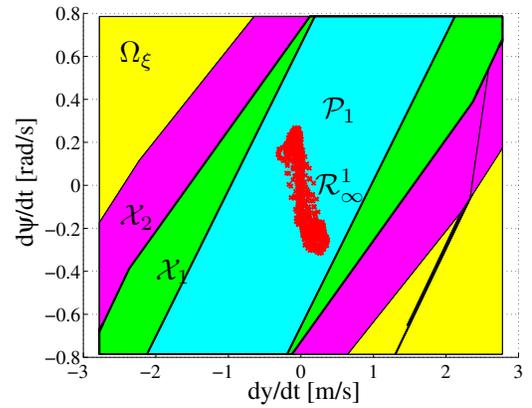
Fig. 5. State Trajectory depicted on $\mathcal{R}_\infty^1$ and 2–step controllable sets $\mathcal{X}_2$ for $\mu = 0.3$ and $40 \leq v_x \leq 50$ [km/h] and vehicle lateral speed [km/h].
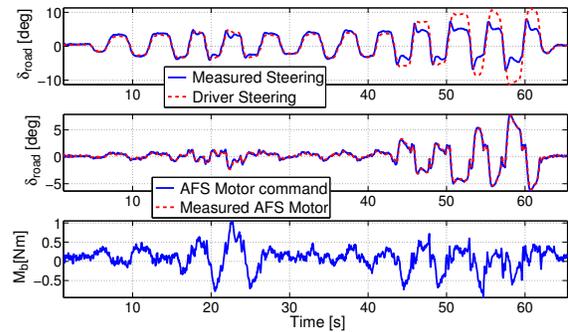
Fig. 6. From the top: a) driver turn wheel angle (dashed line) and real car turn wheel angle; b) AFS Motor command and its experimental measurement; c) Braking Moment command.

with frequency higher than in previous trials and with higher longitudinal acceleration as shown in Figure 7. The response
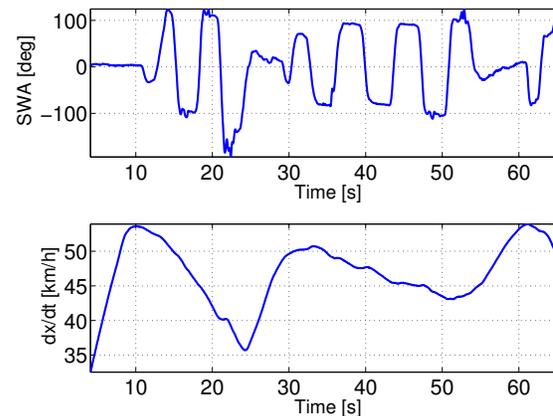
Fig. 7. From the top: driver turn wheel angle δ_d in [deg] and vehicle longitudinal velocity in [km/h]

of the vehicle in this scenario is shown in Figures 8–9. One can see from Figure 8 that the tracking performance is severely impaired. This is due to the excursion of the state trajectory in the region outside the set $\mathcal{R}_\infty^1$ where the

controller's primary objective is not accurate tracking but it is to bring the state vector back to the set $\mathcal{R}_\infty^1$. The state-space plot is shown in Figure 9. In Figure 10 one can see high activity in braking and steering correction as the controller tries to keep the vehicle in the "linear regime" without tire saturations. When the external disturbance eventually drive the state into controllable sets outside $\mathcal{R}_\infty^1$, the controller imposes a large countersteering and braking and restores the stability of the vehicle. The penalty to obtain stability it is an undesired overshoot in yaw rate profile that might be smoothed with a better tuning or including dynamics and constraints of AFS system in the control strategy. This aspect it is confirmed also in Figure 10 where it is evident that the controller is asking for a large steering correction. In some cases this correction cannot be implemented by the AFS (as shown by the difference between the command "motor command" and "measured AFS Motor" signals).
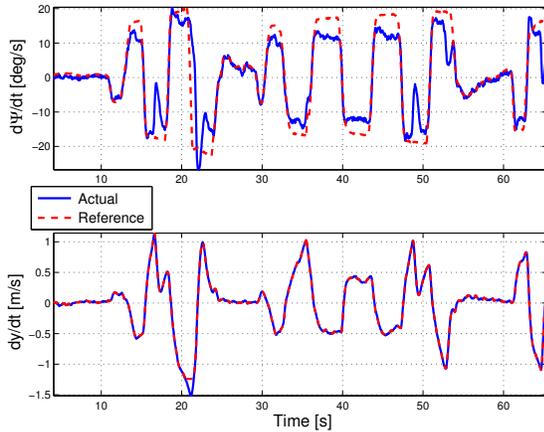
Fig. 8. From the top: a) reference yaw rate (dashed line) and vehicle yaw rate (solid line); b) reference lateral speed (dashed line) and vehicle lateral speed [km/h] .
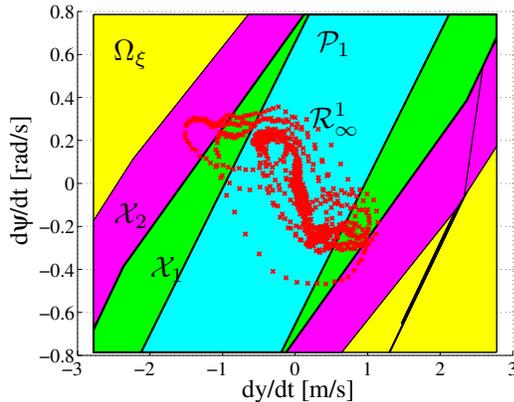
Fig. 9. State Trajectory depicted on $\mathcal{R}_\infty^1$ and 2–step controllable sets $\mathcal{X}_k$ for $\mu = 0.3$ and $40 \leq v_x \leq 50$ [km/h]. and vehicle lateral speed [km/h] .

V. CONCLUSION

In this paper, a vehicle lateral dynamic control approach has been presented utilizing differential braking and active
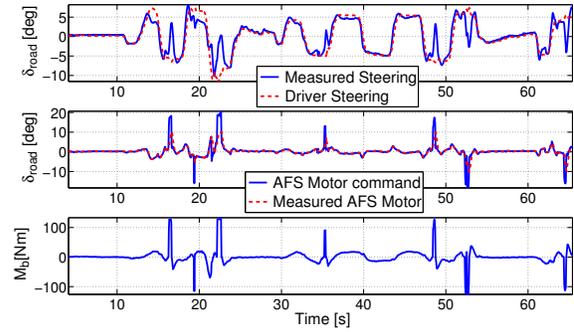
Fig. 10. From the top: a) driver turn wheel angle (dashed line) and real car turn wheel angle; b) AFS Motor command and its experimental measurement; c) Braking Moment command.

front steering. The experimental results prove that the designed controller is able to guarantee constraint satisfaction for longitudinal speed variations. This paper, including other works presented by the same authors ([9], [8], [10]) represent a attempt to address hard constraints and uncertainties in the vehicle stability control system, in a systematic and rigorous way through a robust constrained control design.

VI. ACKNOWLEDGEMENTS

REFERENCES

[1] M. Barić. *Constrained Control: Computations, Performance and Robustness*. PhD thesis, ETH Zürich, 2008.
[2] D. P. Bertsekas. Infinite-time reachability of state-space regions by using feedback control. *IEEE Trans. Automat. Contr.*, 17:604–613, October 1972.
[3] F. Blanchini and S. Miani. *Set-Theoretic Methods in Control*. Birkhäuser, 2008.
[4] P. Falcone, H. E. Tseng, F. Borrelli, J. Asgari, and D. Hrovat. MPC-based yaw and lateral stabilisation via active front steering and braking. *Vehicle System Dynamics*, 46, Supplement:611–628, 2008.
[5] U. Kienke. *Automotive Control Systems*. Springer–Verlag, 2000.
[6] M. Kvasnica, P. Grieder, M. Baotić, and M. Morari. Multi Parametric Toolbox (MPT). In *Hybrid Systems: Computation and Control*. Springer, 2003.
[7] H. B. Pacejka. *Tire and Vehicle Dynamics*. SAE International and Elsevier, 2005.
[8] G. Palmieri, M. Baric, F. Borrelli, and L. Glielmo. Robust eletronic stability controller via set-based methods for uncertain piecewise affine systems. In *18th IFAC World Congress*, 2010.
[9] G. Palmieri, M. Baric, F. Borrelli, and L. Glielmo. A robust lateral vehicle dynamics control. In *10th International Symposium on Advanced Vehicle Control*, 2010.
[10] G. Palmieri, M. Baric, L. Glielmo, and F. Borrelli. Robust vehicle lateral stabilization via set-based methods for uncertain piecewise affine systems. *submitted to Vehicle Dynamics System*, Special Issue, 2011.
[11] R. Rajamani. *Vehicle Dynamics and Control*. Springer–Verlag, 2005.
[12] S. V. Raković, E. C. Kerrigan, D. Q. Mayne, and J. Lygeros. Reachability Analysis of Discrete-Time Systems With Disturbances. *IEEE Trans. Automat. Contr.*, 51(4):546–561, April 2006.
[13] S.V. Raković, M. Barić, and M. Morari. Max-Min Control Problems of Constrained Discrete Time Systems. pages 333–338, Cancun, Mexico, December 2008.